Engineering 17 (2022) 151–160

Contents lists available at ScienceDirect

Engineering

journal homepage: www.elsevier.com/locate/eng

Research
Green Chemical Engineering—Article

An Effective Green Porous Structural Adhesive for Thermal Insulating, Flame-Retardant, and Smoke-Suppressant Expandable Polystyrene Foam

Meng-En Li, Hai-Bo Zhao *, Jin-Bo Cheng, Ting Wang, Teng Fu, Ai-Ning Zhang, Yu-Zhong Wang *

The Collaborative Innovation Center for Eco-Friendly and Fire-Safety Polymeric Materials (MoE) & State Key Laboratory of Polymer Materials Engineering & National Engineering Laboratory of Eco-Friendly Polymeric Materials (Sichuan), College of Chemistry, Sichuan University, Chengdu 610064, China

ARTICLE INFO

Article history:
Received 16 March 2020
Revised 16 June 2020
Accepted 7 August 2020
Available online 18 May 2022

Keywords:
Biomass porous coating
Expanded polystyrene foam
Low thermal conductivity
Flame retardancy
Smoke suppression

ABSTRACT

To develop an efficient way to overcome the contradiction among flame retardancy, smoke suppression, and thermal insulation in expanded polystyrene (EPS) foams, which are widely used insulation materials in buildings, a novel "green" porous bio-based flame-retardant starch (FRS) coating was designed from starch modified with phytic acid (PA) that simultaneously acts as both a flame retardant and an adhesive. This porous FRS coating has open pores, which, in combination with the closed cells formed by EPS beads, create a hierarchically porous structure in FRS–EPS that results in superior thermal insulation with a lower thermal conductivity of 27.0 $mW{\cdot}(m{\cdot}K)^{-1}$. The resultant FRS–EPS foam showed extremely low heat-release rates and smoke-production release, indicating excellent fire retardancy and smoke suppression. The specific optical density was as low as 121, which was 80.6% lower than that of neat EPS, at 624. The FRS–EPS also exhibited self-extinguishing behavior in vertical burning tests and had a high limiting oxygen index (LOI) value of 35.5%. More interestingly, after being burnt with an alcohol lamp for 30 min, the top side temperature of the FRS–EPS remained at only 140 °C with ignition, thereby exhibiting excellent fire resistance. Mechanism analysis confirmed the intumescent action of FRS, which forms a compact phosphorus-rich hybrid barrier, and the phosphorus-containing compounds that formed in the gas phase contributed to the excellent flame retardancy and smoke suppression of FRS–EPS. This novel porous biomass-based FRS system provides a promising strategy for fabricating polymer foams with excellent flame retardancy, smoke suppression, and thermal insulation.

1. Introduction

With the rapid development of urbanization, global energy use has increased greatly. About 40% of the world's total energy consumption comes from maintaining a comfortable interior atmosphere [1]. To reduce unnecessary energy loss, thermal insulation building materials have been developed and play an important part in improving the energy efficiency of buildings [2–5]. Among such materials, expanded polystyrene (EPS) foam occupies the largest market share [6], due to its low cost and density, excellent moisture resistance, shock absorption, and thermal insulation [7–9]. However, as a kind of polyolefin cellular material, EPS is extremely flammable. Moreover, because of its high porosity, large specific surface area, thin pore wall, and air content of as high as 98% (V/V), it is even more difficult for EPS than for its corresponding resin to be made flame-retardant [10,11]. EPS is a significant fire hazard due to its ease of ignition and subsequent rapid flame propagation, heat release, and smoke production [12,13]. As an external insulation building material, EPS has been reported to cause countless fire disasters [14], making it a major potential threat to human lives and properties. Therefore, it is an urgent task to improve the fire safety (including flame retardancy and smoke suppression) of EPS.

Based on the manufacturing process, flame retardants can be added during the polymerization [15–17], foaming [18–22], or post-processing [23] stages to obtain flame-retardant EPS foams. However, the most cost-effective flame retardants used during the polymerization stage are halogen-containing, such as hexabromocyclododecane (HBCD), which has been prohibited by many countries because of serious concerns regarding its bioaccumulation and the toxic substances produced during its thermal degradation [24,25].

* Corresponding authors.
E-mail addresses: haibor7@163.com (H.-B. Zhao), yzwang@scu.edu.cn (Y.-Z. Wang).

https://doi.org/10.1016/j.eng.2020.08.032

Recently, researchers have attempted to coat the surface of EPS beads with halogen-free flame-retardant coatings in order to make fire-safe EPS [18–22]. Each EPS bead, as an independent unit, can be coated with a small number of flame retardants via adhesives to suppress burning. At present, thermosetting resins are usually used as the adhesives in this process, including melamine-formaldehyde and phenolic-formaldehyde resin. However, there is a demand for large amounts of traditional resin adhesives and halogen-free flame retardants due to their low flame-retardant efficiency for EPS, which greatly affects the thermal insulation and other qualities of the foam [26]. Moreover, the use of formaldehyde is harmful to the environment and to the human body [27]. Therefore, it is essential to find an eco-friendly and formaldehyde-free way to improve the flame retardancy and smoke suppression of EPS without sacrificing its thermal insulation.

A "green" biomass-based flame-retardant coating might be the most promising solution to this dilemma, as it would address both health and environmental concerns. More importantly, if a green functional coating could be constructed with a porous microstructure and low thermal conductivity, the contradiction between the flame retardancy and thermal insulation of EPS foam would be solved. Unfortunately, the literature does not contain reports of such a coating.

Inspired by the steaming process of sweet buns and the paste used for pasting spring couplets during the Spring Festival in China, we found that starch, as a natural, renewable, inexpensive, and readily available biopolymer, could be foamed into a porous material when heated and dried [28–31], and has been extensively used as a binder and paste [32,33]. Therefore, we propose the utilization of starch as a green adhesive. In this research, starch is modified by another biomass-based compound, phytic acid (PA) [34–36], via an esterification interaction in order to fabricate a porous flame-retardant starch (FRS), and coat it on the surface of EPS beads. Thus, FRS, which contains starch (a carbon donor and blowing agent) and PA (an acid donor), is used to construct a green intumescent flame-retardant system for EPS foam. This new environmentally friendly approach can endow EPS with superior flame retardancy and smoke suppression, while even improving its thermal insulation due to the hierarchically porous structure of the FRS–EPS foam. The corresponding fire behavior and flame-retardant mechanisms are revealed using integrated methods and are reported here.

2. Experimental methods

2.1. Materials

EPS beads (non-flame-retardant, 0.7–1.1 mm granules, with an expansion ratio of 45–50) were provided by Dongguan Rubber and Plastic Materials Co., Ltd. (China) and were used as control samples. Potato starch (Fig. S1(a) in Appendix A) and PA (Fig. S1(b) in Appendix A) were purchased from Aladdin Industrial Corp. (China). Deionized (DI) water was used throughout, and all materials were used as supplied.

2.2. Sample preparation

EPS beads were first pre-foamed at 110 °C for 8–15 min in an air-circulating oven and then stored at room temperature for 6–12 h. The starch and PA were mixed adequately and then dispersed in a certain amount of DI water. After that, the temperature was raised to 80 °C for about 30 min so that the starch became fully gelatinized. The pre-foamed PS beads were mixed with FRS in a high-speed mixer for at least 30 min. Next, the mixture was transferred into an iron mold at 120 °C under 10 MPa for 6 min to cause the pre-foamed PS beads to expand for the second time, solidify, and fill the shape of the mold. After cooling, the foam boards caused by the mold were taken out and placed in a vacuum oven at 60 °C overnight to ensure that the starch adequately reacted with the PA. The formulation of FRS–EPS is provided in Table S1 in Appendix A, where $E_xS_yPA_z$ refers to the mass ratio (x:y:z) of EPS, starch, and PA, respectively.

2.3. Characterization

Fourier-transform infrared (FT-IR) spectra with a wavenumber ranging from 400 to 4000 cm^{-1} were obtained using an FT-IR spectrometer (Nicolet 170SX, Thermo Fisher Scientific, USA). Thermal gravimetric analysis (TGA) was carried out on a NETZSCH209F1 thermal analyzer (Netzsch, Germany). The samples were heated from 40 to 700 °C under a nitrogen (N_2) and air atmosphere at 10 °C per minute. Thermal gravimetric infrared (TG-IR) spectrometry was conducted to measure the FT-IR spectrum of volatile products at various temperatures with a combination of TGA (NETZSCH209F1) and FT-IR (Nicolet 170SX) from 40 to 700 °C under a nitrogen flow velocity of 50 $mL·min^{-1}$ at 10 °C per minute.

Limiting oxygen index (LOI) tests were conducted following American Society for Testing and Materials (ASTM) D286-97 using an HC-2C oxygen index instrument; at least three samples with the dimensions of 150 mm × 10 mm × 10 mm were used. Vertical burning tests for the FRS–EPS and neat EPS were carried out on a CZF-2 instrument (China) with a UL-94 standard according to ASTM D3801. The samples were the same size as those used in the LOI tests. Cone calorimeter (CC) tests were applied to measure the combustion behavior of the samples using a CC instrument (FTT, UK) with an external heat flux of 35 $kW·m^{-2}$, according to ISO 5660-1:2015. The sample dimensions were 100 mm × 100 mm × 20 mm. Optical density tests were conducted in a smoke density chamber at 25 $kW·m^{-2}$ according to ISO 5659-2:2006. The dimensions of the samples used for the tests were 75 mm × 75 mm × 20 mm.

The morphologies of FRS–EPS and the char residues remaining after the CC tests were analyzed by means of scanning electron microscopy (SEM; JSM 5900LV, JEOL, Japan) with an acceleration voltage of 20 kV. The FRS–EPS samples were fractured in liquid nitrogen to maintain their original morphology. The elemental analysis results for the char residues were measured using an energy-dispersive X-ray (EDX) spectrometer (INCA Oxford Instruments, UK).

Three-dimensional (3D) topographical images and surface roughness were determined by means of laser scanning confocal microscopy (LSCM; LSM800, Carl Zeiss AG, Germany). The X-ray photoelectron spectroscopy (XPS) curves of the char residue from FRS–EPS after the CC tests were obtained using an XSAM80 spectrometer (Kratos Co., UK) with an Al Ka excitation radiation (hv-1486.6 eV, 1 eV = 1.602176 × 10^{-19} J). Raman spectroscopy was measured with a LabRAM HR800 laser Raman spectrometer (Horiba Ltd., Japan) with a 532 nm helium–neon laser line. The thermal conductivities for FRS–EPS and neat EPS (30 mm × 30 mm × 10 mm) were measured with a Hot Disk 2500-OT (Hot Disk, Sweden) according to ISO 22007-2:2008. The mechanical properties of FRS–EPS and neat EPS were determined by means of an electronic universal testing machine (3366, Instron Co. Ltd., USA) according to ISO 845:2004. The average value of at least five samples' stress at 10% deformation was taken as the compressive strength of the foam; the dimensions for all the samples were 50 mm × 50 mm × 20 mm. The densities of the FRS–EPS and neat EPS were measured at room temperature according to ISO 845:2006. More than three samples with the dimensions of 100 mm × 100 mm × 20 mm were measured in order to obtain average values.

3. Results and discussion

3.1. Reaction between starch and PA

The flame-retardant coating, FRS, was fabricated from PA and starch. A PA molecule contains six phosphate groups, allowing it to react with the hydroxyl groups in starch. Fig. 1 shows the proposed mechanism for the reaction between starch and PA. In brief, starch reacts with PA to construct a cross-linked network, accompanied by the formation of a phosphonate ester bond [37]. As PA possesses abundant phosphorus (P), it endows the EPS with excellent flame-retardant properties. To illustrate the proposed reaction between PA and starch and to characterize the chemical structure of the FRS, FT-IR and XPS analysis were conducted. As shown in Fig. 2(a), a new absorption peak at 1037 cm^{-1} was observed for FRS, which was assigned to C–O–P [38]. Furthermore, the width narrowed and the intensity decreased around 3400 cm^{-1}, indicating that the incorporation of PA destroyed the intramolecular hydrogen bonds of the starch. The XPS results revealed P 2s and P 2p for S4PA4, and the O 2s of starch moved to a higher energy level, further denoting that the starch reacted with PA to form FRS.

3.2. Cell morphology

To investigate the effects of the FRS coating on the cell morphology of EPS, SEM measurements were conducted. SEM images of neat EPS, E8S4, and E8S4PA1 are shown in Fig. 3. In general, the neat EPS foam displays a closed-cell structure with a smooth surface, with some spaces existing among the spherical cells (Fig. 3(a)). Under the adhesion of starch, a porous coating covers the closed cells and fills in the interspace (Fig. 3(b)), which may explain why the starch precursor after gelatinization retains its porous structure under ambient drying [28–31,39,40]. More interestingly, as shown in Fig. 3(c), E8S4PA1 exhibits a uniform porous coating with open pores on the large EPS spheres, creating a hierarchically porous structure. That is, after the starch is modified with PA, the porous FRS structure becomes more uniform and more open pores are present, probably due to the cross-linking action between PA and starch. This increases the skeleton strength and keeps the network skeleton from collapsing during the drying process, allowing the porous structure to be maintained [31].

Confocal laser scanning microscope tests for neat EPS and FRS–EPS were further conducted to investigate the morphology and

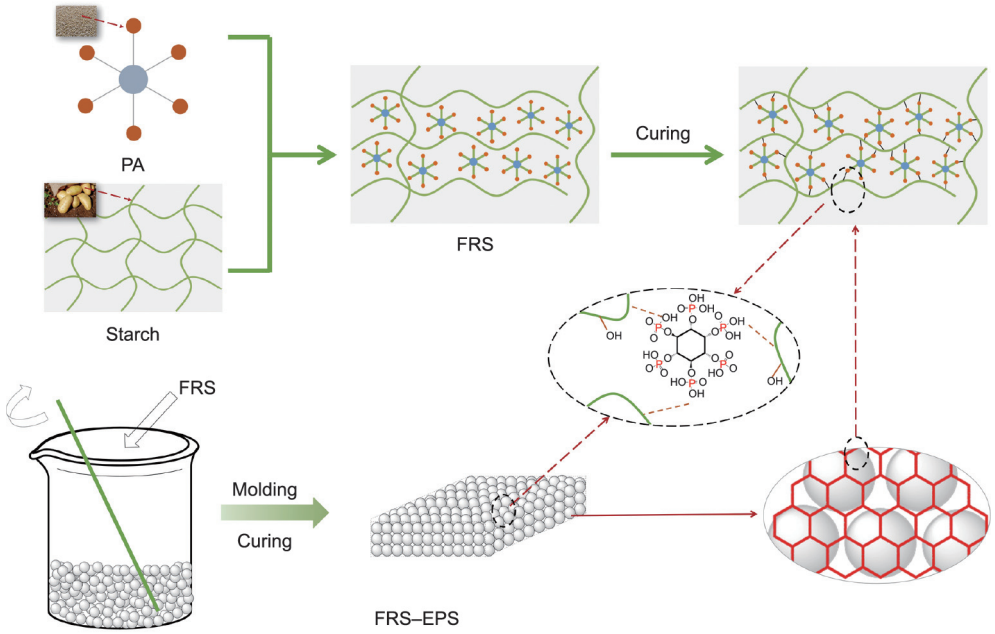

Fig. 1. Preparation process of FRS and FRS–EPS.

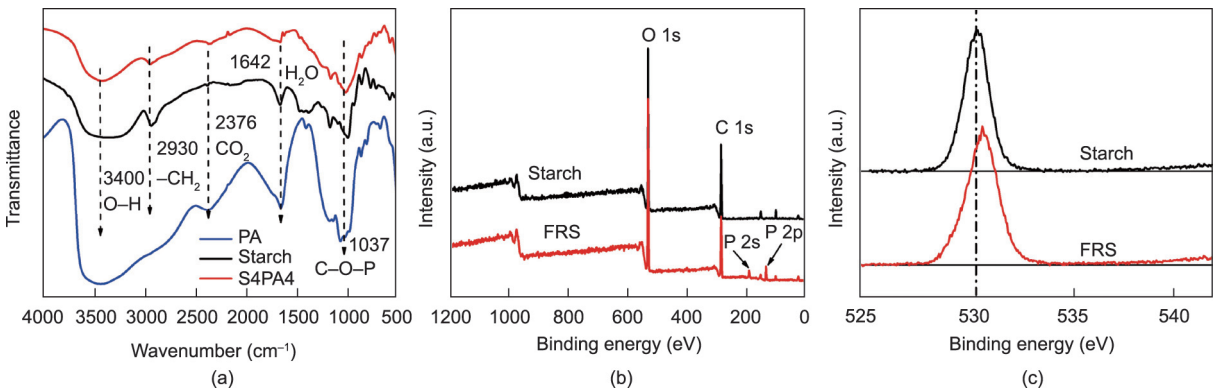

Fig. 2. (a) FT-IR spectra of S4PA4, starch, and PA; (b) XPS spectra; and (c) O 2s spectra of starch and FRS.

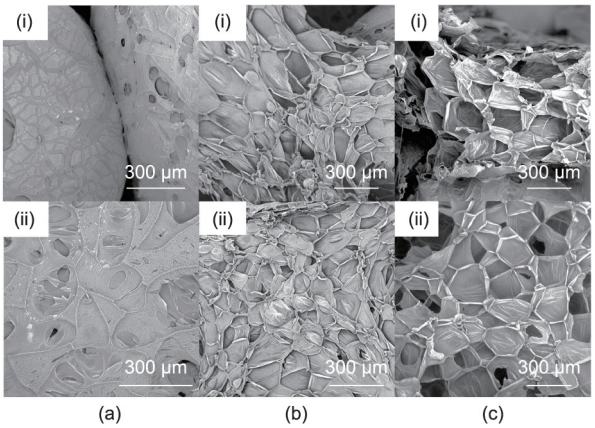

Fig. 3. SEM images of (a) neat EPS, (b) E8S4, and (c) E8S4PA1.

surface roughness. As shown in Fig. S2 in Appendix A, the surface roughness of an EPS bead coated with S4PA1 increased from 85.7 to 156.0 μm for the neat EPS bead, and significant differences in cup depth were detected on the bead for E8S4PA1, further indicating the presence of an open porous coating on the EPS bead. In addition, the FRS was evenly and tightly coated onto the EPS beads without separation between the beads. This hierarchically porous structure plays a key role in improving the thermal insulation of the FRS–EPS foam.

3.3. Physical behavior

The physical behavior of EPS, including its mechanical properties and thermal insulation, are very important in its real applications, especially in the field of building insulation. The corresponding data of FRS–EPS and neat EPS are shown in Fig. 4. As shown in Fig. 4(a), the compressive strength of the neat EPS was 157 kPa, while that of the FRS–EPS increased greatly. In particular, E8S4PA4 showed the highest compressive strength at 313 kPa, which was 200% that of neat EPS. Due to the closed-cell structure of EPS, the FRS was coated on the cell wall of the EPS beads. With an increasing concentration of FRS precursors, the coating became harder and stronger, resulting in a higher compressive strength of FRS–EPS. When the PA content was too high in the coating, the compressive strength of the foam decreased slightly, probably because the excessive PA destroyed the adhesiveness of the FRS.

More interestingly, the incorporation of the FRS coating did not result in a higher thermal conductivity, as was previously reported for traditional flame-retardant EPS foam with a resin coating [26]. On the contrary, the thermal conductivity decreased from 30.3 $mW·(m·K)^{-1}$ for neat EPS to 27.0 $mW·(m·K)^{-1}$ for E8S4PA1, with a reduction of 10.9% (Fig. 4(b)), indicating that the FRS coating improves the thermal insulation of EPS. This result can be ascribed to the porous structure of the FRS coating. As shown in Fig. 3, compared with the simple closed-cell structure of neat EPS (Fig. 3(a)), FRS–EPS has a hierarchically porous structure with closed cells due to the EPS and open pores due to the FRS, which contribute to a decrease in thermal conductivity [3].

IR thermal imaging tests were further conducted to demonstrate the excellent thermal insulation capability of FRS–EPS. Fig. 5 depicts pseudo-color thermal images and the time-dependent temperature curves for the upper surfaces of E8S4PA1 and neat EPS samples with a thickness of 2 cm during continuous heating on a 100 °C heater. As shown in Fig. 5, when heated at the same time, the temperatures of the upper surface points of E8S4PA1 were always much lower than those of the neat EPS, demonstrating the much better thermal insulation provided by the former. Remarkably, the temperature of an upper surface point of E8S4PA1 only increased from 25.7 to 29.5 °C after being heated at 100 °C for 60 min. Clearly, placing a porous FRS coating onto EPS effectively improves its thermal insulation.

3.4. Thermal stability

The thermal stability of FRS–EPS and neat EPS were investigated by means of TGA (Fig. 6), and the corresponding data are summarized in Table 1. Neat EPS had only one decomposition stage from 400 to 470 °C and there was almost no residue after thermal degradation. In contrast, a two-step degradation process was observed in FRS–EPS, which was ascribed to the respective degradation of FRS and EPS. The FRS coating decomposed in the first stage from 130 to 400 °C to form a protective char layer, thereby reducing the mass loss rate to a certain extent. As seen in Table 1, the maximum degradation temperature (T_{max}) of the FRS–EPS increased slightly while the corresponding mass loss rate decreased greatly in comparison with those of neat EPS, indicating that the char layer that formed in the first stage of FRS degradation slowed down the degradation of EPS. The T_{max} and loss rate for E8S4PA8 were 444.7 °C and −9.82% per minute, respectively. Furthermore, the charring ability of FRS–EPS was gradually enhanced with an increasing PA content, with E8S4PA8 having the highest residue (32.60%). This finding indicates that PA promotes the formation of more char. The char layer acts as a protective barrier to effectively prevent further degradation of EPS, thus improving the flame retardancy of FRS–EPS.

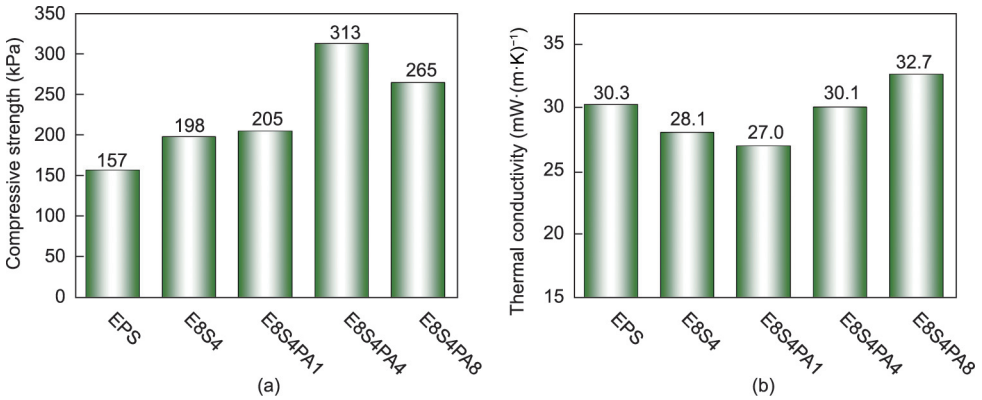

Fig. 4. (a) Compressive strength and (b) thermal conductivity of FRS–EPS and neat EPS.

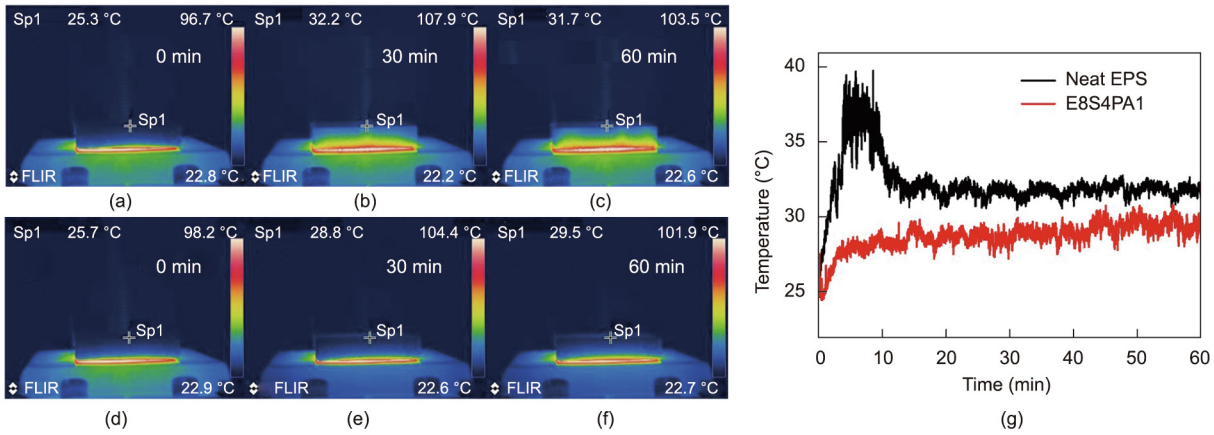

Fig. 5. Thermal insulation of FRS–EPS and neat EPS samples with a thickness of 2 cm during continuous heating on a 100 °C heater. Pseudo-color thermal images at different time points from 0 to 60 min: (a–c) neat EPS; (d–f) E8S4PA1. (g) Time-dependent temperature curves of the upper surface points (Sp).

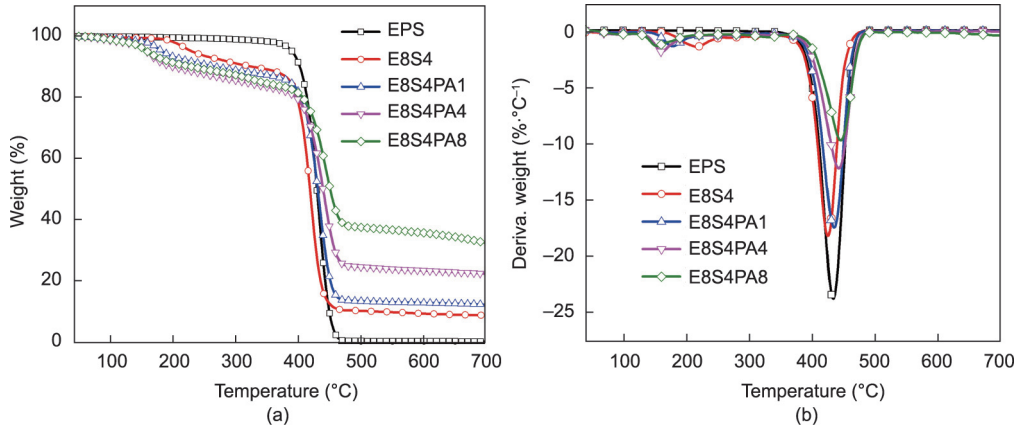

Fig. 6. (a) TGA and (b) derivative thermogravimetry (DTG) curves for FRS–EPS and neat EPS at a heating rate of 10 °C per minute in N_2.

Table 1
Characteristic TGA data of FRS–EPS and neat EPS at a heating rate of 10 °C per minute in N_2.

Sample	$T_{5\%}$ (°C)	T_{max} (°C)	Max loss rate (% per minute)	Residue at 700 °C (%)
EPS	391.0	432.8	−23.89	0.45
E8S4	231.8	420.7	−21.10	8.98
E8S4PA1	184.2	434.4	−17.55	12.49
E8S4PA4	159.2	441.7	−12.32	22.58
E8S4PA8	159.8	444.7	−9.82	32.60

$T_{5\%}$: temperature of 5% weight loss.

3.5. Combustion behavior

3.5.1. Small fire tests

LOI and vertical burning tests are classic small fire tests, which were used to evaluate the fire safety of FRS–EPS. As shown in Table 2, neat EPS was extremely flammable, with a very low LOI value of only 17.0%, while the introduction of the FRS coating significantly improved the flame retardancy of the foam. It was found that the LOI values of the foam increased gradually with increasing PA content. Notably, E8S4PA8 showed the highest LOI value of 35.5%.

The vertical burning tests of FRS–EPS and neat EPS are shown in Fig. 7 and the results are listed in Table 2. Neat EPS burnt completely with serious dripping and spread to the fixture as it ignited (left side of Fig. 7), while E8S4 failed to pass the tests. With the incorporation of PA-modified starch, the FRS–EPS passed the V-0 rank without dripping during combustion. In particular, E8S4PA8 exhibited self-extinguishing behavior (center right of Fig. 7) and could not be ignited a second time (far right of Fig. 7), showing excellent small-fire safety performance.

3.5.2. Fire resistance

The fire resistance of the foam was evaluated by means of alcohol lamp burning tests. An alcohol lamp was used to impart a continuous high-temperature flame to E8S4PA8 and neat EPS samples with a thickness of 2 cm, and the corresponding thermal images were recorded. As shown in Fig. 8, when neat EPS was exposed to the alcohol lamp, the fire quickly spread to the top of the sample along with a considerable amount of smoke production, and the backside surface temperature reached a maximum of 325 °C in just 20 s. As the EPS combustibles burnt out, the temperature gradually decreased. In contrast, a compact char shielding formed on the surface of E8S4PA8, which effectively suppressed the combustion and fire spreading. Even after being continuously burnt for 30 min, the

Table 2
UL-94 and LOI tests of FRS–EPS and neat EPS.

Sample	UL-94	LOI (%)
Neat EPS	N.R.	17.0
E8S4	N.R.	20.0
E8S4PA1	V-2	23.0
E8S4PA4	V-1	28.5
E8S4PA8	V-0	35.5

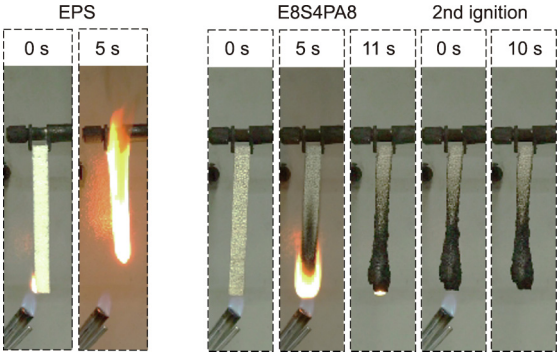

Fig. 7. Digital photos of neat EPS and E8S4PA8 during vertical burning tests.

FRS–EPS prevented the flame from burning through the backside surface and maintained its structural integrity. More interestingly, the temperature at the center of the backside surface increased slowly and stabilized at 140 °C after being burnt for 15 min. It was notable that the temperature at the edge of the top surface was actually maintained at the original room temperature, indicating superior high-temperature thermal insulation. These results demonstrate that FRS–EPS meets the strict demands for high-temperature thermal insulation and fire resistance.

3.5.3. Large-scale combustion and smoke-suppressant behavior

The CC test is an effective method to evaluate the large-scale combustion behavior of materials. It yields key parameters, including the peak heat-release rate (PHRR), total heat release (THR), peak smoke-production rate (PSPR), and total smoke production (TSP), which can be used to predict the fire and smoke hazards of a material in a real fire [41–45]. Curves for the abovementioned parameters are presented in Figs. 9 and 10, and the corresponding detailed data are provided in Table 3. Lower PHRR and THR values indicate that a lesser amount of heat is released during a fire. It was found that the PHRR value of neat EPS reached 640 kW·m^{-2}, while E8S4 had an even higher value of 683 kW·m^{-2}; however, the incorporation of FRS greatly decreased the PHRR value. The PHRR value of E8S4PA8 was only 107 kW·m^{-2}, which was 83.3% less than that of neat EPS. Thus, FRS acts as an effective protective barrier to restrict the fire spread rate. The THR value showed the same trend as the PHRR value, with the THR value of E8S4PA8 (4.7 MJ·m^{-2}) being 83.1% less than that of neat EPS (27.8 MJ·m^{-2}). This result further confirms the effective combustion inhibition of FRS.

Lower PSPR and TSP values denote a lower smoke risk and a longer escape time during a fire. As shown in Fig. 10 and Table 3, the incorporation of FRS greatly reduced the smoke emission of EPS. The PSPR value of E8S4PA8 was only 0.10 m^2·s^{-1}, which was much lower than that of neat EPS at 0.37 m^2·s^{-1}, demonstrating that FRS acts as an effective protective layer to slow down smoke release. The TSP values also decreased significantly with the incorporation of FRS. The TSP value of E8S4PA8 was as low as 4.1 m^2, which was 78.9% lower than that of neat EPS (19.4 m^2). This excellent smoke-suppressant performance may be due to the improved charring ability of FRS, which was also indicated by the residue values after the CC tests. The residue from E8S4PA8 was 73%, which was much greater than that of E8S4 (5 wt%) or neat EPS (0). During combustion, FRS promotes the formation of char layers to prohibit smoke emission.

Smoke density chamber tests were further conducted to evaluate the smoke-release behavior of FRS–EPS and neat EPS. A high transmission value reflects high visibility, which indicates more chances to escape in a fire. As shown in Fig. 11(a), neat EPS burnt acutely during combustion with a very low transmission (almost 0), and the incorporation of starch did not improve the transmission. However, after the starch was modified with PA, it increased the transmission greatly: The transmission of E8S4PA4 was as high as 12.5%, which was much higher than that of neat EPS (0%). The smoke density directly corresponds to the smoke hazard of the materials in a fire. As shown in Fig. 11(b), the specific optical density (D_s) of neat EPS tended to stabilize around 624 after 150 s,

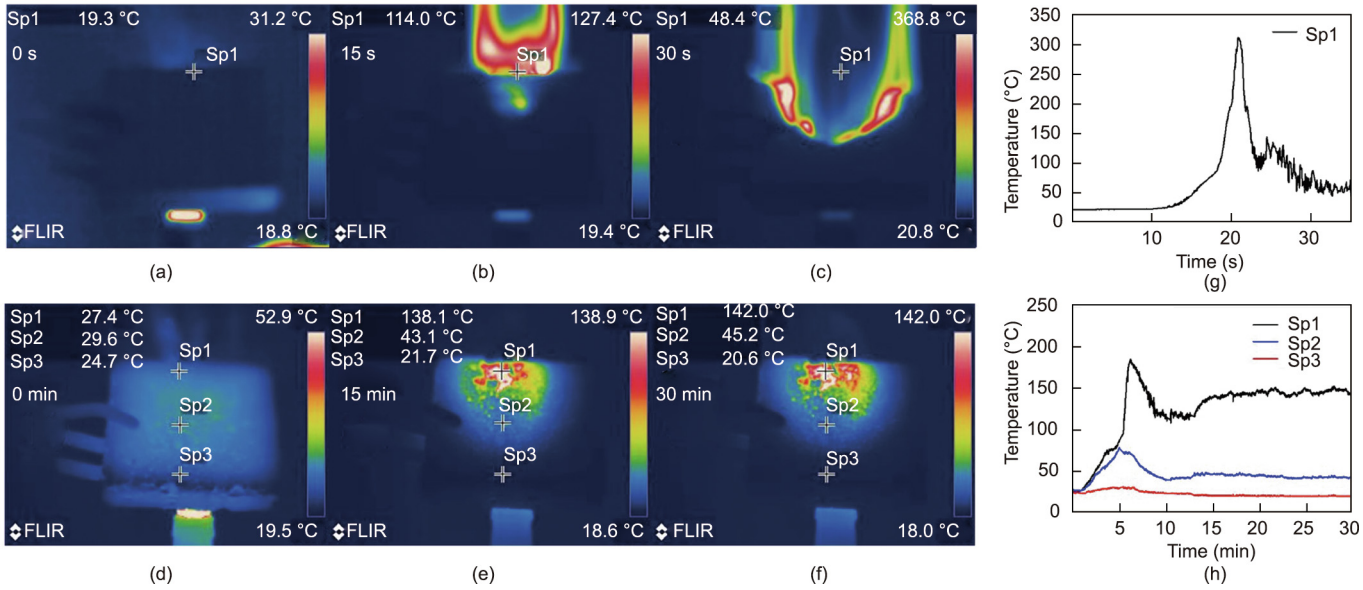

Fig. 8. Pseudo-color thermal images during alcohol lamp burning tests for (a–c) neat EPS and (d–f) E8S4PA8. The corresponding time-dependent temperature curves of the backside surface points for (g) neat EPS and (h) E8S4PA8.

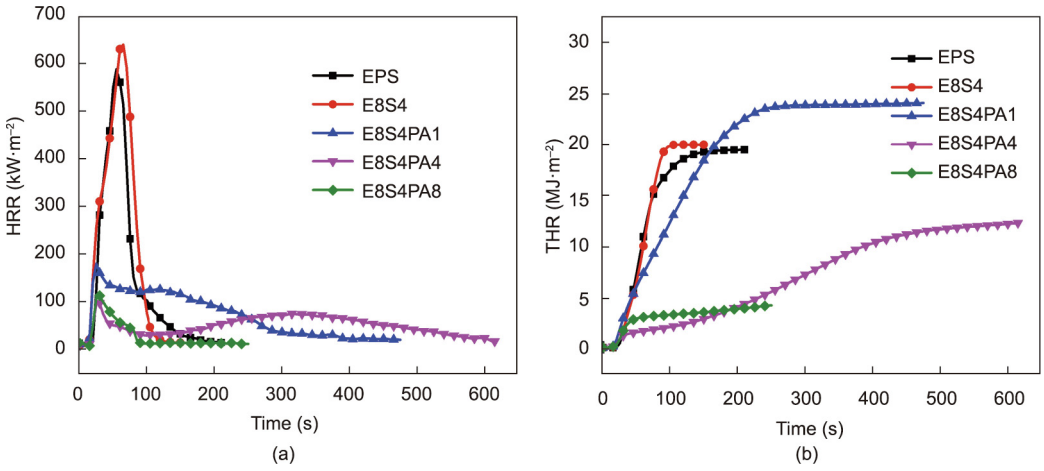

Fig. 9. (a) Heat-release rate (HRR) curves and (b) THR curves for FRS–EPS and neat EPS during CC tests under 35 kW·m^{-2}.

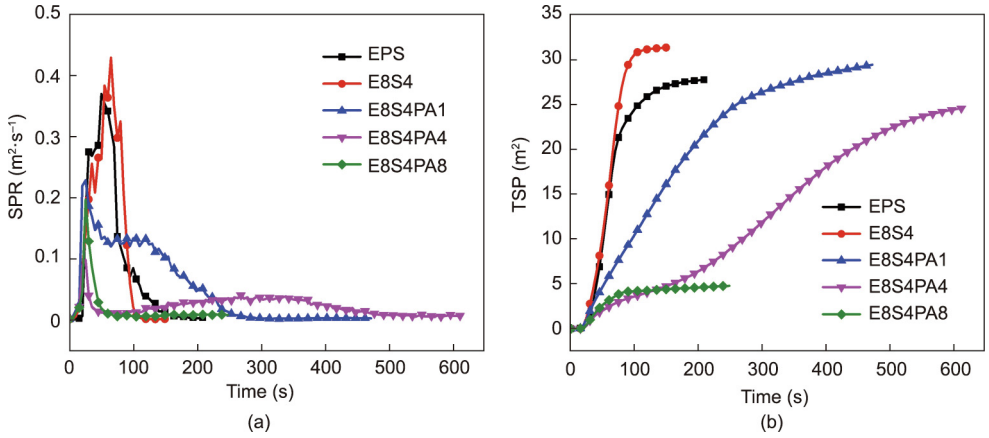

Fig. 10. (a) Smoke-production rate (SPR) curves and (b) TSP curves for FRS–EPS and neat EPS during CC tests under 35 kW·m^{-2}.

Table 3
Characteristic data for FRS–EPS and neat EPS during CC tests under 35 kW·m^{-2}.

Samples	TTI (s)	PHRR (kW·m^{-2})	THR (MJ·m^{-2})	FIGRE (kW·m^{-2}·s^{-1})	PSPR (m^2·s^{-1})	TSP (m^2)	Residue (%)
EPS	12	640	27.8	9.1	0.37	19.4	0
E8S4	14	683	31.2	9.8	0.35	19.9	5
E8S4PA1	15	173	29.4	5.7	0.23	24.0	17
E8S4PA4	12	181	24.6	5.5	0.19	12.2	41
E8S4PA8	18	107	4.7	3.5	0.10	4.1	73

TTI: time to ignite; FIGRE: the ratio of PHRR to TPHRR (time to PHRR).

while E8S4 showed a much greater specific density of 670. Fortunately, the starch modified with PA effectively reduced the smoke density of EPS: The specific optical density of E8S4PA4 was as low as 121, which was 80.6% lower than that of neat EPS, at 624. It was obvious that the biomass-based FRS coating endowed the EPS with excellent smoke-suppressant ability.

3.6. Flame-retardant and smoke-suppressant mechanism

To investigate the flame-retardant and smoke-suppressant mechanism of FRS, TG-IR was used to study the gaseous products during the thermal degradation of FRS–EPS. Fig. 12 shows the IR spectra of the volatilized products at typical degradation temperatures for neat EPS, E8S4, and E8S4PA4, respectively. As shown in Fig. 12(a) and Fig. 6, the degradation of neat EPS occurred at 400 °C. The absorption peaks at 1625 and 3050 cm^{-1} were attributed to the skeletal vibration of the benzene ring and to =C–H stretching vibrations, respectively, indicating that EPS mainly degraded into aromatic monomers, dimers, aromatic heterocyclic groups, and so on. No residue was left and the real-time absorption peak disappeared at 504 °C. As shown in Fig. 12(b), new characteristic peaks at 1120 and 1300 cm^{-1} appeared at 405 °C for E8S4, which were assigned to the vibration of C–O and O–H from the decomposition of starch. For E8S4PA4, a new peak at 1000 cm^{-1}, which was attributed to C–O–P, was observed at 419 °C. Furthermore, the peak at 3050 cm^{-1} was much lower than those of neat

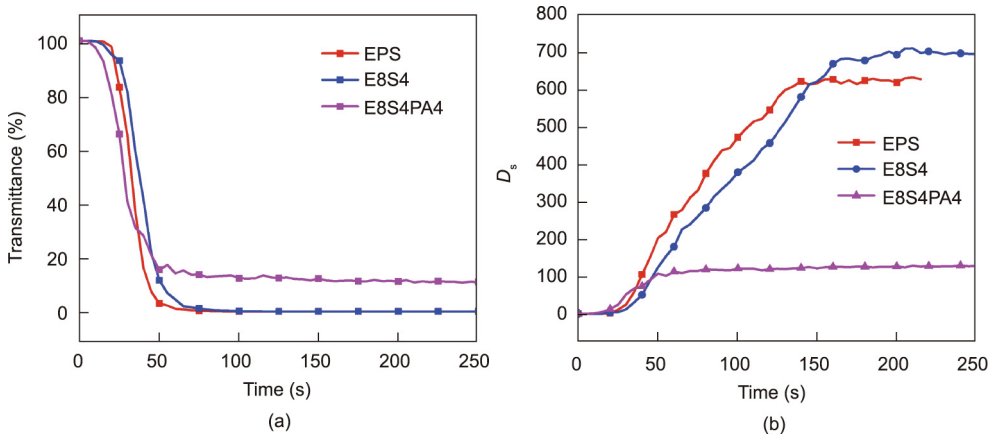

Fig. 11. (a) Light transmission and (b) specific optical density (D_s) curves for FRS–EPS and neat EPS with a pilot flame at 25 kW·m^{-2}.

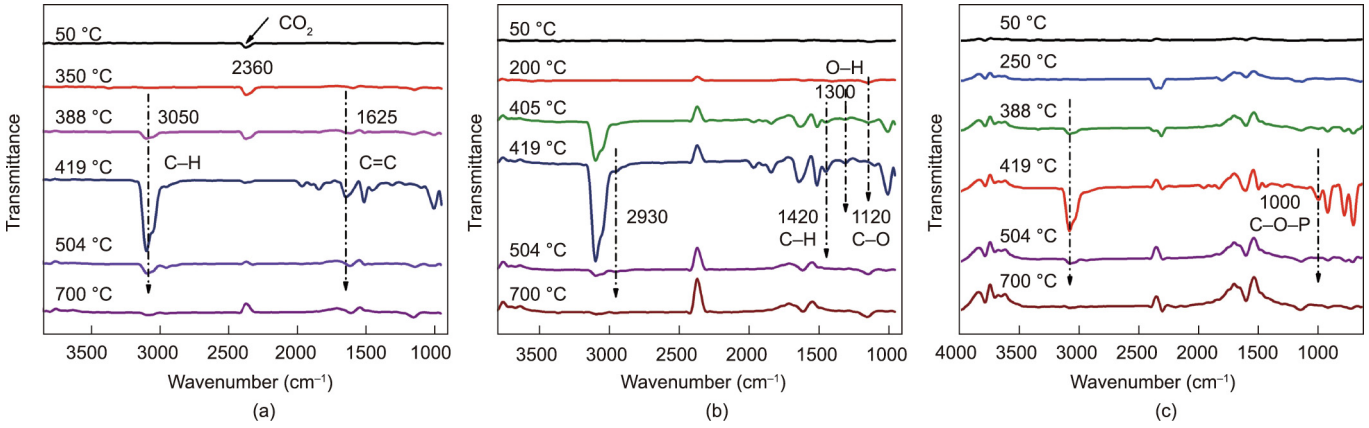

Fig. 12. FT-IR spectra of the decomposition products of (a) neat EPS, (b) E8S4, and (c) E8S4PA4 at characteristic thermal degradation temperatures.

EPS and E8S4, and the absorption peak at 1625 cm^{-1} still existed at 700 °C, which was due to the FRS slowing down the decomposition of EPS. Therefore, it can be concluded that FRS not only slows down the decomposition of EPS, but also generates noncombustible phosphorous compounds to dilute the oxygen and combustible volatile gases in the combustion area, thus playing an important role in gas-phase flame retardation.

Fig. S3 in Appendix A and Fig. 13 show the digital photos and SEM images of the residual char after CC tests. As shown in Fig. S3, almost no residual char was left by neat EPS and E8S4, while obvious intumescent carbon layers were observed for E8S4PA4 and E8S4PA8. Also, a dense and continuous char residue was displayed by FRS–EPS (Fig. 13). With increasing PA content in the coating, the microstructures of the char residue became more compact. Few defects were found for the intumescent carbon layers of E8S4PA4, indicating the best protection effect. It was speculated that PA promoted the formation of phosphorus-rich compact char layers, resulting in a better flame retardancy for EPS. To verify this hypothesis, EDX spectrometry, FT-IR, and XPS were conducted to study the elemental composition and chemical structure of the residue after CC tests. As shown in Appendix A Figs. S4 and S5, the absorption peaks around 1000 cm^{-1}, which were assigned to C–O–P, existed in all the residues of FRS–EPS in the FT-IR spectra, and P 2s and P 2p peaks were observed in the XPS spectra.

Raman tests were further conducted to characterize the degree of graphitization of the char residue after combustion. As shown in Fig. 14, the peak at 1368 cm^{-1}, called the D band, is associated with amorphous disordered carbon, while the peak at 1590 cm^{-1}, assigned to the G band, is related to the graphitized char layer with sp^2 hybridized carbon [46–48]. The degree of graphitization of the residual char is demonstrated by the D and G band intensity ratio (I_D/I_G). A lower I_D/I_G denotes a greater degree of graphitization, resulting in more stable char structures and better flame retardancy. As shown in Fig. 14, the I_D/I_G of FRS–EPS decreased gradually with increasing PA content. Thus, PA acts as a catalyst to promote the graphitization of the char, resulting in the formation of a more stable phosphorus-rich hybrid char that endows EPS with better flame retardancy.

Overall, the flame-retardant and smoke-suppressant mechanism of FRS–EPS can be speculated, as shown in Fig. 15. When FRS–EPS is burnt, the starch in the coating quickly dehydrates under PA catalysis to form a carbon skeleton. Then the nonflammable gases (e.g., CO_2, H_2O, and P-containing compounds) generated during the decomposition of FRS blow up the carbon scaffold to form an intumescent, compact, and stable phosphorus-rich hybrid char layer. This hybrid char layer acts as a protective barrier to suppress the emission of combustible gases and smoke, and inhibit the transportation of heat, oxygen, and other thermal degradation products to the surface. Furthermore, the non-flammable gases dilute the oxygen concentration and prevent combustible volatile gases from entering the combustion area. Under the condensed and gaseous phase action of FRS, FRS–EPS exhibits an outstanding flame-retardant, fire-resistant, and smoke-suppressant performance.

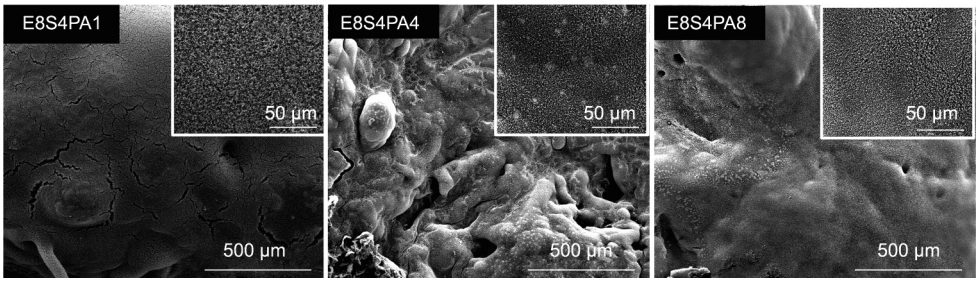

Fig. 13. SEM images of char residues from FRS–EPS after CC tests.

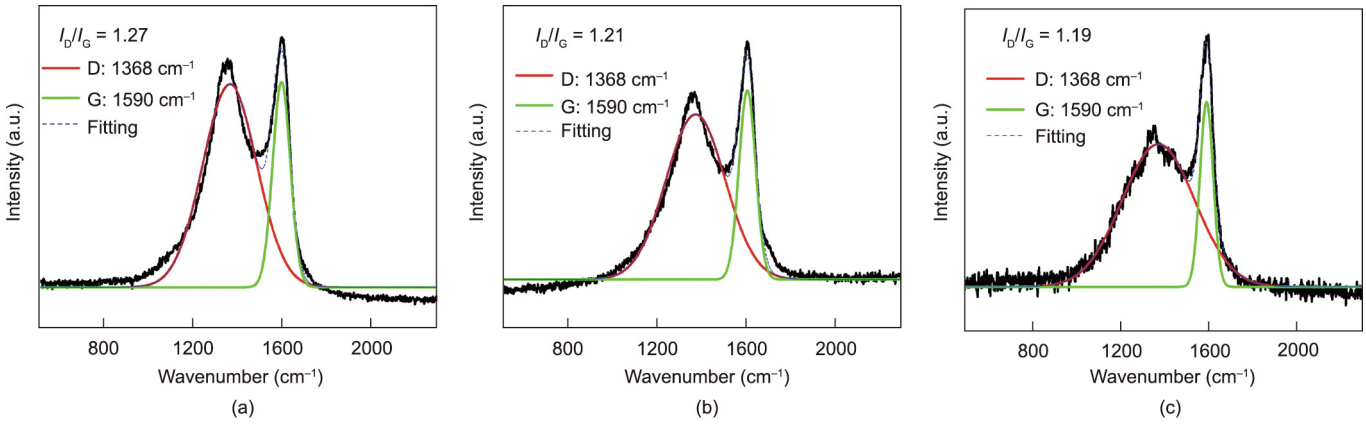

Fig. 14. Raman spectra for the char residues after the CC tests of (a) E8S4PA1, (b) E8S4PA4, and (c) E8S4PA8, respectively.

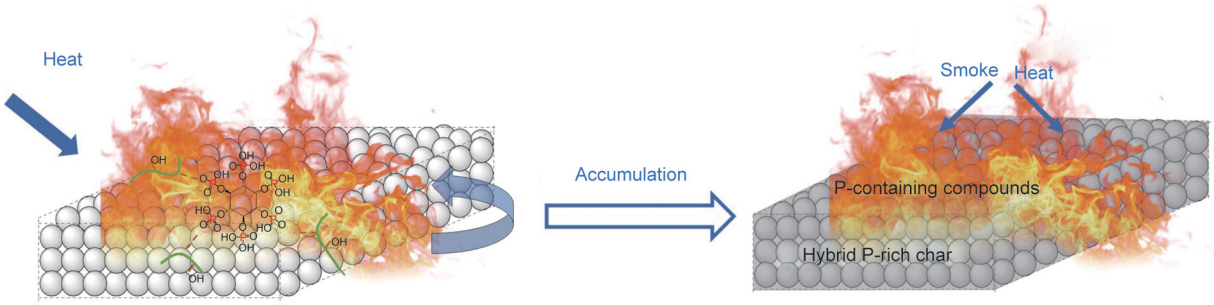

Fig. 15. Flame-retardant and smoke-suppressant mechanism model diagram of FRS–EPS.

4. Conclusions

In summary, a novel green porous FRS coating obtained from starch modified with PA was designed and decorated onto EPS beads, resulting in highly efficient thermal insulating, flame-retardant, and smoke-suppressant foams. Benefiting from the porous structure of FRS, the resultant foam exhibited a decreased thermal conductivity of 27.0 $mW·(m·K)^{-1}$. The FRS also greatly improved the compressive strength while reducing the flammability and smoke emission of the EPS. In particular, the FRS–EPS was able to retain its original shape without ignition after being burnt with an alcohol lamp for 30 min; it also effectively restricted heat transfer, exhibiting excellent high-temperature thermal insulation. TG-IR, SEM, and Raman results confirmed that a compact and stable phosphorus-rich hybrid barrier and phosphorus-containing compounds in the gas phase contributed to the excellent flame retardancy and smoke suppression. This work provides a new green approach to solve the contradiction between fire safety and thermal insulation for EPS foam. The obtained foams exhibit the combined advantages of high fire resistance, smoke suppression, and low thermal conductivity, thereby demonstrating great potential for building insulation.

Acknowledgments

This work was financially supported by the National Natural Science Foundation of China (51827803, 51320105011, 51790504, and 51721091), the Young Elite Scientists Sponsorship Program by CAST, and Fundamental Research Funds for the Central Universities.

Compliance with ethics guidelines

Meng-En Li, Hai-Bo Zhao, Jin-Bo Cheng, Ting Wang, Teng Fu, Ai-Ning Zhang, and Yu-Zhong Wang declare that they have no conflict of interest or financial conflicts to disclose.

Appendix A. Supplementary data

Supplementary data to this article can be found online at https://doi.org/10.1016/j.eng.2020.08.032.

References

[1] Široký J, Oldewurtel F, Cigler J, Prívara S. Experimental analysis of model predictive control for an energy efficient building heating system. Appl Energy 2011;88(9):3079–87.
[2] Cao ZJ, Liao W, Wang SX, Zhao HB, Wang YZ. Polyurethane foams with functionalized graphene towards high fire-resistance, low smoke release, superior thermal insulation. Chem Eng J 2019;361:1245–54.
[3] Li ME, Wang SX, Han LX, Yuan WJ, Cheng JB, Zhang AN, et al. Hierarchically porous SiO_2/polyurethane foam composites towards excellent thermal insulating, flame-retardant and smoke-suppressant performances. J Hazard Mater 2019;375:61–9.
[4] Wang SX, Zhao HB, Rao WH, Huang SC, Wang T, Liao W, et al. Inherently flame-retardant rigid polyurethane foams with excellent thermal insulation and mechanical properties. Polymer 2018;153:616–25.
[5] Chen HB, Shen P, Chen MJ, Zhao HB, Schiraldi DA. Highly efficient flame retardant polyurethane foam with alginate/clay aerogel coating. ACS Appl Mater Interfaces 2016;8(47):32557–64.
[6] Xu Q, Jin C, Griffin G, Jiang Y. Fire safety evaluation of expanded polystyrene foam by multi-scale methods. J Therm Anal Calorim 2014;115(2):1651–60.
[7] Raps D, Hossieny N, Park CB, Altstädt V. Past and present developments in polymer bead foams and bead foaming technology. Polymer 2015;56:5–19.
[8] Wang J, Chow W. A brief review on fire retardants for polymeric foams. J Appl Polym Sci 2005;97(1):366–76.
[9] Tian HZ, Zhu CY, Gao JJ, Cheng K, Hao JM, Wang K, et al. Quantitative assessment of atmospheric emissions of toxic heavy metals from anthropogenic sources in China: historical trend, spatial distribution, uncertainties, and control policies. Atmos Chem Phys 2015;15(17):10127–47.
[10] Zhang H, Kuo YY, Gerecke AC, Wang J. Co-release of hexabromocyclododecane (HBCD) and nano- and microparticles from thermal cutting of polystyrene foams. Environ Sci Technol 2012;46(20):10990–6.
[11] Hong Y, Fang X, Yao D. Processing of composite polystyrene foam with a honeycomb structure. Polym Eng Sci 2015;55(7):1494–503.
[12] Yu B, Liu M, Lu L, Dong X, Gao W, Tang K. Fire hazard evaluation of thermoplastics based on analytic hierarchy process (AHP) method. Fire Mater 2010;34(5):251–60.
[13] Zhou K, Gui Z, Hu Y. The influence of graphene based smoke suppression agents on reduced fire hazards of polystyrene composites. Compos Part A Appl Sci Manuf 2016;80:217–27.
[14] Stec AA, Hull TR. Assessment of the fire toxicity of building insulation materials. Energy Build 2011;43(2–3):498–506.
[15] Glück G, Dietzen FJ, Hahn K, Ehrmann G, inventors. Method for producing expandable polystyrene particles. United States patent 6444714 B1. 2002.
[16] Levchik SV, Weil ED. New developments in flame retardancy of styrene thermoplastics and foams. Polym Int 2008;57(3):431–48.
[17] Huang J, Zhao Z, Chen T, Zhu Y, Lv Z, Gong X, et al. Preparation of highly dispersed expandable graphite/polystyrene composite foam via suspension polymerization with enhanced fire retardation. Carbon 2019;146:503–12.
[18] Zhang S, Ji W, Han Y, Gu X, Li H, Sun J. Flame-retardant expandable polystyrene foams coated with ethanediol-modified melamine–formaldehyde resin and microencapsulated ammonium polyphosphate. J Appl Polym Sci 2018;135(28):46471–8.
[19] Cao Bo, Gu X, Song X, Jin X, Liu X, Liu X, et al. The flammability of expandable polystyrene foams coated with melamine modified urea formaldehyde resin. J Appl Polym Sci 2017;134(5):44423–30.
[20] Wang Z, Jiang S, Sun H. Expanded polystyrene foams containing ammonium polyphosphate and nano-zirconia with improved flame retardancy and mechanical properties. Iran Polym J 2017;26(1):71–9.
[21] Sayadi AA, Tapia JV, Neitzert TR, Clifton GC. Effects of expanded polystyrene (EPS) particles on fire resistance, thermal conductivity and compressive strength of foamed concrete. Constr Build Mater 2016;112:716–24.
[22] Zhu ZM, Xu YJ, Liao W, Xu SM, Wang YZ. Highly flame retardant expanded polystyrene foams from phosphorus–nitrogen–silicon synergistic adhesives. Ind Eng Chem Res 2017;56(16):4649–58.
[23] Hamdani-Devarennes S, El Hage R, Dumazert L, Sonnier R, Ferry L, Lopez-Cuesta JM, et al. Water-based flame retardant coating using nano-boehmite for expanded polystyrene (EPS) foam. Prog Org Coat 2016;99:32–46.
[24] Messer A. Mini-review: polybrominated diphenyl ether (PBDE) flame retardants as potential autism risk factors. Physiol Behav 2010;100(3):245–9.
[25] Covaci A, Gerecke AC, Law RJ, Voorspoels S, Kohler M, Heeb NV, et al. Hexabromocyclododecanes (HBCDs) in the environment and humans: a review. Environ Sci Technol 2006;40(12):3679–88.
[26] Li ME, Yan YW, Zhao HB, Jian RK, Wang YZ. A facile and efficient flame-retardant and smoke-suppressant resin coating for expanded polystyrene foams. Compos Part B Eng 2020;185:107797–803.
[27] Li X, Chen H, Wang W, Liu Y, Zhao P. Synthesis of a formaldehyde-free phosphorus–nitrogen flame retardant with multiple reactive groups and its application in cotton fabrics. Polym Degrad Stabil 2015;120:193–202.
[28] Zhao S, Malfait WJ, Guerrero-Alburquerque N, Koebel MM, Nyström G. Biopolymer aerogels and foams: chemistry, properties, and applications. Angew Chem Int Ed 2018;57(26):7580–608.
[29] Bergel BF, Dias Osorio S, da Luz LM, Santana RMC. Effects of hydrophobized starches on thermoplastic starch foams made from potato starch. Carbohydr Polym 2018;200:106–14.
[30] Soykeabkaew N, Thanomsilp C, Suwantong O. A review: starch-based composite foams. Compos Part A Appl Sci Manuf 2015;78:246–63.
[31] Shogren R, Lawton J, Doane W, Tiefenbacher K. Structure and morphology of baked starch foams. Polymer 1998;39(25):6649–55.
[32] Wang Z, Li Z, Gu Z, Hong Y, Cheng L. Preparation, characterization and properties of starch-based wood adhesive. Carbohydr Polym 2012;88(2):699–706.
[33] Zhang Y, Ding L, Gu J, Tan H, Zhu L. Preparation and properties of a starch-based wood adhesive with high bonding strength and water resistance. Carbohyd Polym 2015;115:32–7.
[34] Guo Q, Cao J, Han Y, Tang Y, Zhang X, Lu C. Biological phytic acid as a multifunctional curing agent for elastomers: towards skin-touchable and flame retardant electronic sensors. Green Chem 2017;19(14):3418–27.
[35] Cheng XW, Liang CX, Guan JP, Yang XH, Tang RC. Flame retardant and hydrophobic properties of novel sol-gel derived phytic acid/silica hybrid organic–inorganic coatings for silk fabric. Appl Surf Sci 2018;427:69–80.
[36] Wang PJ, Liao DJ, Hu XP, Pan N, Li WX, Wang DY, et al. Facile fabrication of biobased PNC-containing nano-layered hybrid: preparation, growth mechanism and its efficient fire retardancy in epoxy. Polym Degrad Stabil 2019;159:153–62.
[37] Zhao Y, Li XN, Chen T, Tang QY, Qiu LY, Wang BJ, et al. Preparation and antioxidant activity of phosphorylated polysaccharides from *Russula alutacea* Fr. Ekoloji 2018;27(105):17–22.
[38] Rupper P, Gaan S, Salimova V, Heuberger M. Characterization of chars obtained from cellulose treated with phosphoramidate flame retardants. J Anal Appl Pyrolysis 2010;87(1):93–8.
[39] Chang X, Chen D, Jiao X. Starch-derived carbon aerogels with high-performance for sorption of cationic dyes. Polymer 2010;51(16):3801–7.
[40] Wang Y, Wu K, Xiao M, Riffat SB, Su Y, Jiang F. Thermal conductivity, structure and mechanical properties of konjac glucomannan/starch based aerogel strengthened by wheat straw. Carbohydr Polym 2018;197:284–91.
[41] Wang YT, Zhao HB, Degracia K, Han LX, Sun H, Sun M, et al. Green approach to improving the strength and flame retardancy of poly(vinyl alcohol)/clay aerogels: incorporating biobased gelatin. ACS Appl Mater Interfaces 2017;9(48):42258–65.
[42] Rao WH, Zhu ZM, Wang SX, Wang T, Tan Y, Liao W, et al. A reactive phosphorus-containing polyol incorporated into flexible polyurethane foam: self-extinguishing behavior and mechanism. Polym Degrad Stabil 2018;153:192–200.
[43] Liu BW, Chen L, Guo D, Liu X, Lei Y, Ding X, et al. Fire-safe polyesters enabled by end-group capturing chemistry. Angew Chem Int Ed 2019;58(27):9188–93.
[44] Fu T, Zhao X, Chen L, Wu W, Zhao Q, Wang XL, et al. Bioinspired color changing molecular sensor toward early fire detection based on transformation of phthalonitrile to phthalocyanine. Adv Funct Mater 2019;29(8):1806586.
[45] Li P, Wang B, Xu YJ, Jiang Z, Dong C, Liu Y, et al. Ecofriendly flame-retardant cotton fabrics: preparation, flame retardancy, thermal degradation properties, and mechanism. ACS Sustain Chem Eng 2019;7(23):19246–56.
[46] Peng H, Wang D, Fu S. Tannic acid-assisted green exfoliation and functionalization of MoS_2 nanosheets: significantly improve the mechanical and flame-retardant properties of polyacrylonitrile composite fibers. Chem Eng J 2020;384:123288.
[47] Zhao HB, Cheng JB, Wang YZ. Biomass-derived Co@crystalline carbon@carbon aerogel composite with enhanced thermal stability and strong microwave absorption performance. J Alloys Compd 2018;736:71–9.
[48] Jian RK, Ai YF, Xia L, Zhao LJ, Zhao HB. Single component phosphamide-based intumescent flame retardant with potential reactivity towards low flammability and smoke epoxy resins. J Hazard Mater 2019;371:529–39.